ADVANCED MATERIALS

centrifugation and/or dialysis against de-ionized water. Microgel particles had dimensions of ca. 220 nm (pH 3.92, $T = 25\,^{\circ}C$) and polydispersity of ca. 4 % measured by photon correlation spectroscopy (Zeta-sizer 3000, Malvern, UK).

Prior to the synthesis of photoluminescent Ag nanoclusters, the microgel dispersion (3 mL) was treated with a 0.1 M aqueous solution of KOH to adjust the value of pH to the desired value. Then 0.4 ml of a freshly prepared 0.2 M $AgNO_3$ solution was introduced into the dispersion and the final volume was adjusted to 4 ml by adding the de-ionized water. The concentration of silver ions [Ag^+] in the microgel dispersion was 0.01 M. The Ag^+ ion–microgel dispersion was stirred for 30 min, dialyzed for 2 days against de-ionized water, and then subjected to UV irradiation for various time intervals.

Photoluminescence of hybrid microgels was studied by using spectrofluorometry (Photon Technology International, Inc.). Light from a tungsten–halogen lamp was directed into a monochromator. The outgoing excitation ($\lambda_{ex} = 450$ nm) was passed through a low-pass filter (to eliminate higher orders of diffraction) and focused onto the microgel dispersion. A lens was used to collect the photoluminescence and direct it onto the slit of a second monochromator, which was coupled to a photomultiplier for visible signal detection.

Received: May 24, 2005
Final version: July 12, 2005
Published online: August 22, 2005

[1] a) C. B. Murray, D. J. Norris, M. G. Bawendi, *J. Am. Chem. Soc.* **1993**, *115*, 8706; b) M. Bruchez, M. Moronne, P. Gin, S. Weiss, A. P. Alivisatos, *Science* **1998**, *281*, 2013; c) W. C. W. Chan, S. Nie, *Science* **1998**, *281*, 2016; d) M. P. Pileni, *Adv. Funct. Mater.* **2001**, *11*, 323; e) Y. G. Sun, Y. Xia, *Science* **2002**, *298*, 2176.

[2] a) C. Burda, X. Chen, R. Narayanan, M. A. El-Say, *Chem. Rev.* **2005**, *105*, 1025; b) P. V. Kamat, *J. Phys. Chem. B* **2002**, *106*, 7729.

[3] L. A. Peyser, A. E. Vinson, A. P. Bartko, R. M. Dickson, *Science* **2001**, *291*, 103.

[4] a) J. Zheng, R. M. Dickson, *J. Am. Chem. Soc.* **2002**, *124*, 13 982; b) J. Zheng, J. T. Petty, R. M. Dickson, *J. Am. Chem. Soc.* **2003**, *125*, 7780; c) J. Zheng, C. W. Zhang, R. M. Dickson, *Phys. Rev. Lett.* **2004**, *93*, 0 77402; d) J. T. Petty, J. Zheng, N. V. Hud, R. M. Dickson, *J. Am. Chem. Soc.* **2004**, *126*, 5207.

[5] a) J. P. Wilcoxon, J. E. Martin, *J. Chem. Phys.* **1998**, *108*, 9137; b) L. A. Peyser, T.-H. Lee, R. M. Dickson, *J. Phys. Chem. B* **2002**, *106*, 7725.

[6] a) G. B. Ershov, A. B. Henglein, *J. Phys. Chem. B* **1998**, *102*, 10 663; b) A. Henglein, M. Giersig, *J. Phys. Chem. B* **1999**, *103*, 9533.

[7] D. G. Shchukin, I. L. Radtchenko, G. B. Sukhorukov, *ChemPhysChem* **2003**, *4*, 1101.

[8] a) W. Funke, O. Okay, B. Joos-Muller, *Adv. Polym. Sci.* **1998**, *136*, 138; b) Z. Hu, X. Zhang, Y. Li, *Science* **1995**, *269*, 525.

[9] a) S. Xu, J. Zhang, C. Paquet, Y. Lin, E. Kumacheva, *Adv. Funct. Mater.* **2003**, *13*, 468; b) L. A. Lyon, J. D. Debord, S. B. Debord, C. D. Jones, J. G. McGrath, M. J. Serpe, *J. Phys. Chem. B* **2004**, *108*, 19 099.

[10] a) J. Zhang, S. Xu, E. Kumacheva, *J. Am. Chem. Soc.* **2004**, *126*, 7908; b) S. Xu, J. Zhang, E. Kumacheva, *Compos. Interfaces* **2003**, *10*, 405.

[11] M. Mostafavi, N. Keghouche, M. O. Delcourt, J. Belloni, *Chem. Phys. Lett.* **1990**, *167*, 193.

[12] a) M. P. Mallin, C. J. Murphy, *Nano Lett.* **2002**, *2*, 1235; b) A. Slistan-Grijalva, R. Herrera-Urbina, J. F. Rivas-Silva, M. Avalos-Borja, F. F. Catillon-Barraza, A. Posada-Amarillas, *Physica E (Amsterdam, Neth.)* **2005**, *27*, 104.

[13] A. Henglein, *J. Phys. Chem.* **1993**, *97*, 5457.

[14] a) I. Rabin, W. Schulze, G. Ertl, *Chem. Phys. Lett.* **1999**, *312*, 394; b) V. Bonacic-Koutecky, V. Veyret, R. Mitric, *J. Chem. Phys.* **2001**, *115*, 10 450.

[15] S. Eustis, H.-Y. Hsu, M. A. El-Sayed, *J. Phys. Chem. B* **2005**, *109*, 4811.

[16] *X-ray Diffraction Procedures* (Eds.: H. P. Klug, L. E. Alexander), John Wiley and Sons, New York **1959**.

[17] W. I. Lee, Y. Bae, A. J. Bard, *J. Am. Chem. Soc.* **2004**, *126*, 8358.

[18] K. Malone, S. Weaver, D. Taylor, H. Cheng, K. P. Sarathy, G. Mills, *J. Phys. Chem. B* **2002**, *106*, 7422.

[19] *Encyclopedia of Polymer Science and Engineering*, 2nd ed. (Ed: J. I. Kroschwitz), John Wiley and Sons, New York **1985**, p. 212.

[20] *Lang's Handbook of Chemistry*, 15th ed. (Ed: J. A. Dean), MacGraw–Hill, New York **1999**, p. 332.

[21] N. Kashyap, N. Kumar, M. N. V. R. Kumar, *Crit. Rev. Ther. Drug Carrier Syst.* **2005**, *22*, 107.

[22] a) S. Nayak, H. Lee, J. Chmielewski, L. A. Lyon, *J. Am. Chem. Soc.* **2004**, *126*, 10 258; b) I. Gorelikov, L. Field, E. Kumacheva, *J. Am. Chem. Soc.* **2004**, *126*, 15 938.

Direct Correlation of Organic Semiconductor Film Structure to Field-Effect Mobility**

By *Dean M. DeLongchamp*,* *Sharadha Sambasivan*, *Daniel A. Fischer*, *Eric K. Lin*, *Paul Chang*, *Amanda R. Murphy*, *Jean M. J. Fréchet*, and *Vivek Subramanian*

New devices and applications have emerged with the development of organic electronic materials amenable to high-volume manufacturing, incorporation on flexible substrates, and designed functionality. Technologies under development in-

[*] Dr. D. M. DeLongchamp, E. K. Lin
Polymers Division of the Materials Science and Engineering Laboratory
National Institute of Standards and Technology
Gaithersburg, MD 20899 (USA)
E-mail: dean.delongchamp@nist.gov
S. Sambasivan, D. A. Fischer
Ceramics Division of the Materials Science and Engineering Laboratory
National Institute of Standards and Technology
Gaithersburg, MD 20899 (USA)
P. Chang, Prof. V. Subramanian
Department of Electrical Engineering and Computer Sciences
University of California
Berkeley, CA 94720 (USA)
A. R. Murphy, Prof. J. M. J. Fréchet
Department of Chemistry
University of California
Berkeley, CA 94720 (USA)

[**] Official contribution of the National Institute of Standards and Technology; not subject to copyright in the United States. D. M. D. acknowledges the NIST/NRC postdoctoral program. The authors gratefully acknowledge funding from DOE-BES, AFOSR, and MARCO. Certain equipment, instruments or materials are identified in this paper in order to adequately specify the experimental details. Such identification does not imply recommendation by the National Institute of Standards and Technology nor does it imply the materials are necessarily the best available for the purpose.

  DOI: 10.1002/adma.200500263

clude printable large-area displays, wearable electronics, electronic paper, low-cost photovoltaic cells, sensors, and radio-frequency identification tags. New materials and processes are evolving rapidly to optimize device performance, ease processing limitations, and demonstrate frontier applications. In particular, tremendous effort has been directed towards solution-based processing strategies where fabrication in ambient conditions is possible.[1–4]

Significant progress has been made towards formulations for inkjet printing, spin-coating, or dip-coating. However, establishing direct correlations between the material structure and device performance has been challenging. These challenges are exemplified in recently developed soluble precursor molecules that thermally convert into high-performance organic semiconductors.[5–8] Conversion of precursor films involves changes in structure at many levels. First, the chemical structure changes as solubilizing groups are removed. Simultaneously, the molecules reorient with respect to the substrate. Finally, this large-scale molecular reorganization causes the film to become thinner, eventually reaching monolayer and submonolayer coverage. Each of these changes strongly impacts the performance of the semiconductor as an active layer in organic field-effect transistors (OFETs).

Techniques such as atomic force microscopy (AFM) and grazing-incidence X-ray diffraction (GIXD) provide structural information that has been correlated to OFET performance. However, these techniques each provide a different aspect of structural characterization. AFM is a local probe of nanometer-scale heterogeneity, and GIXD is a non-local measurement of unit-cell dimensions and preferential orientation relative to the substrate for crystalline regions. A single measurement that unambiguously quantifies chemical composition, orientation, and defects for broad classes of organic semiconductor films (amorphous or crystalline) would enhance the rational development of new materials and processes.

Here we demonstrate the use of near-edge X-ray absorption fine structure (NEXAFS) spectroscopy to track the effects of thermal processing on the chemistry and structure of oligothiophene precursor films. NEXAFS is a nondestructive, synchrotron-based spectroscopic method in which soft X-rays are absorbed, causing resonant excitations of core K- or L-shell electrons to unoccupied (antibonding) molecular orbitals. The polarized soft X-rays can be exploited to measure bond orientation within a film.[9] The detector choice also provides selective measurement of either the near surface or film bulk.[10,11] NEXAFS spectroscopy is ideally suited to organic semiconductors due to its sensitivity to π-bonds, its insensitivity to roughness, and its ability to probe films from <1 nm to 100 nm thick.

In this work, NEXAFS measurements are used for a detailed investigation of the structural evolution of nanoscale films during the thermal conversion of a solution-processable oligothiophene that has exhibited high p-type mobilities in OFET devices. Large variations in field-effect hole mobility, as shown in Figure 1a, are directly correlated to the quantified

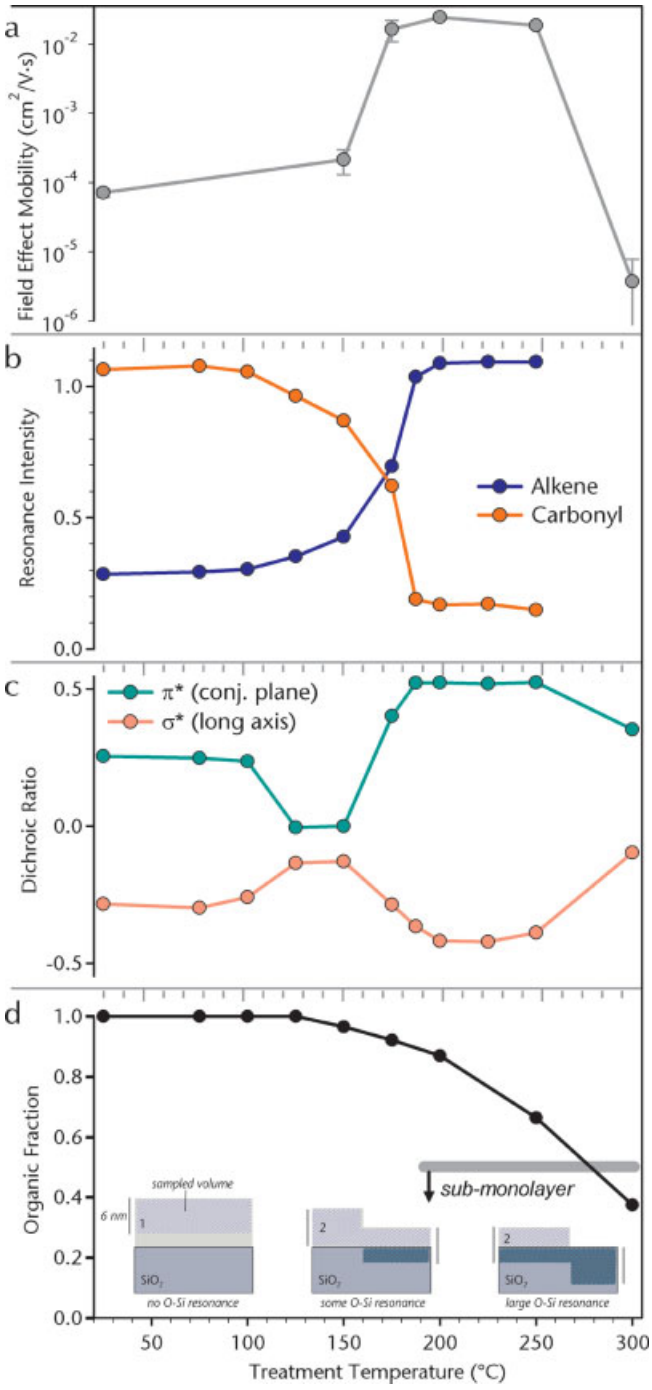

Figure 1. a) Development of field-effect hole mobility with increasing treatment temperature. b) Integrated peak intensities quantifying the increasing density of alkene bonds and decreasing density of carbonyl bonds within the sampling volume. c) Dichroic ratios of the sexithiophene core in films of **1** and **2** (see Fig. 2) at various stages of thermal treatment. d) Organic fraction within sampling volume calculated from the oxygen-silicon σ* resonance of the SiO_2 dielectric from films of **1** and **2** at increasing treatment temperatures. Inset images depict the probed depth in thin films.

orientation and distribution of molecules (Figs. 1b–d). The oligothiophene precursor is the symmetric diester-functionalized sexithiophene derivative **1** containing activated second-

ADVANCED MATERIALS

ary esters, as shown in Figure 2a.[7] Thermolysis of the esters in the bulk state is initiated at treatment temperatures greater than 175 °C, which converts the precursor into the symmetric sexithiophene **2** with pendant alkylene groups. Films of **1** were

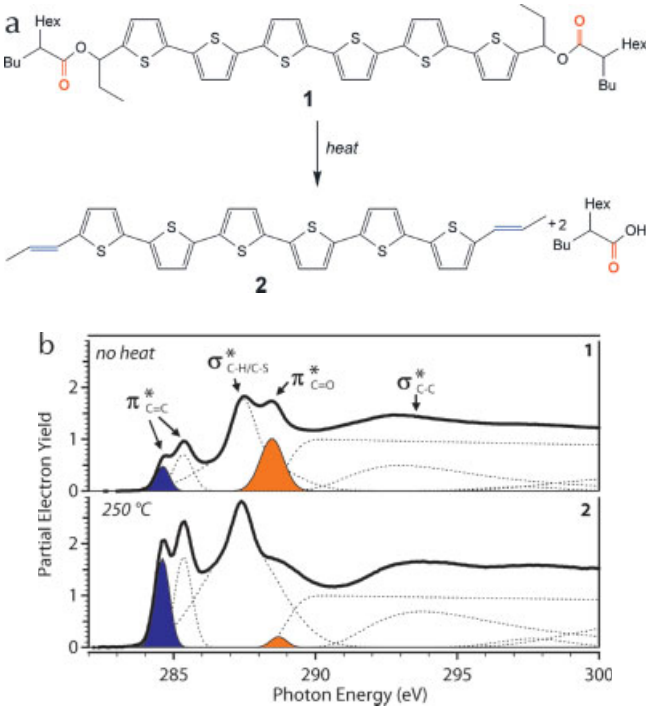

Figure 2. a) Chemical structures of the soluble precursor **1** and the product **2** after thermolysis. Bu indicates butyl groups and Hex indicates hexyl groups. b) Carbon K-edge NEXAFS spectra before and after thermolysis of the esters. The blue resonance is the alkene, while the orange resonance is the carbonyl. Spectra are collected with soft X-rays incident at the orientation-insensitive "magic" angle, 54.7°, and are normalized to the total carbon surface signal. Experimental standard uncertainty in peak position for partial electron yield (PEY) mode spectra is ±0.1 eV; yield uncertainty is ±2 %.

spin-cast from chloroform (2–3 mg mL^{-1} solutions) on a 100 nm SiO_2 dielectric thermally grown on highly n-doped silicon. A thermal treatment series was created by heating films to temperatures between 75 °C and 300 °C for 20 min and then cooling them to room temperature.

NEXAFS spectroscopy was performed at the NIST/Dow soft X-ray materials characterization facility at the National Synchrotron Light Source (NSLS) of Brookhaven National Laboratory. Carbon K-edge spectra were collected in PEY mode with a sampling depth of 6 nm. As-cast films of **1** are approximately 20 nm thick. We expect the conversion, orientation, and defects within the sampling volume to closely match the mobile channel region closest to the dielectric layer.[12]

To quantify chemical conversion, spectra were collected for the entire temperature-treatment sample series. Representative spectra are shown in Figure 2b. We assign the lowest-energy resonance at 284.7 eV to 1 s → carbon–carbon π* excitations of the pendant alkenes on **2**, and the 285.4 eV resonance to the 1 s → carbon–carbon π* of the thiophene rings.[13–15] The 288.5 eV peak is the carbon–oxygen σ* resonance of the ester and acid byproduct carbonyls.[16] The resonance at 287.5 eV is the sum of carbon–hydrogen and carbon–sulfur σ* excitations, and the three peaks above 290 eV are carbon–carbon σ* resonances.

Resonances are quantified by fitting a combination of peak shapes to the spectra and then integrating peak areas. The results are shown in Figure 1b. Thermolysis is quantified by the increasing alkene resonance, along with a simultaneous decrease in carbonyl resonance due to acid evaporation. Alkene intensity is observed even in unheated films, indicating some minor conversion of the nominal precursor. Conversion in these thin films is initiated at lower temperatures than observed in bulk samples,[7] possibly due to acid catalysis by SiO_2. Thermolysis is complete at 200 °C, which can be further confirmed by oxygen K-edge scans. The ester carbonyl resonance at 532.4 eV[16] decreases with heating, but a small acid carbonyl resonance at 531.0 eV[16] remains constant up to 250 °C, finally disappearing at 300 °C. Even though conversion to the dialkene is complete at 200 °C, a small quantity of trapped acid remains within the film at temperatures up to 300 °C.

Molecular orientation can also be quantified with NEXAFS by evaluating the angular dependence of carbon spectra. The carbon–carbon π*- and σ*-resonant intensities (Fig. 3a) exhibit a strong angular dependence that corresponds to a dipole defined by the spatial orientation of the final state orbital. The π* resonance is a vector normal to the conjugated plane, while the σ* resonance is a vector (primarily) along the long axis (Fig. 3b). Intensity will be proportional to the squared cosine of the angle between the incident electric field vector and the resonance vector. The π* intensity is largest at normal incidence (90°), indicating that the conjugated plane of **2** tilts away from the substrate in an "edge-on" orientation. The σ* intensity is greatest at glancing incidence (20°), indicating that the long axis of **2** is normal to the substrate in a "standing-up" orientation. These independent measurements of planar and long-axis tilt support a self-consistent orientation that is depicted in Figure 3b.

The changes in molecular orientation that accompany thermolysis can be quantified using a dichroic ratio, *R*, defined in Figure 3b.[17,18] Intensity at 0° incidence was extrapolated from five incident angles, with a minor correction for electron-yield loss.[19] The *R* for the orientation of the molecular plane was based on the sexithiophene π* resonance, while the *R* for long-axis orientation was based on the first σ* resonance at 294 eV. *R* can vary between +0.75 and –1.00, where a more-positive *R* for the conjugated plane indicates increased tilt away from the substrate, while a more-negative *R* for the long axis indicates greater surface normality.

We observe four distinct orientation regimes in Figure 1c. First, the precursor **1** is vertically oriented even when unconverted, and this weak orientation persists until the treatment

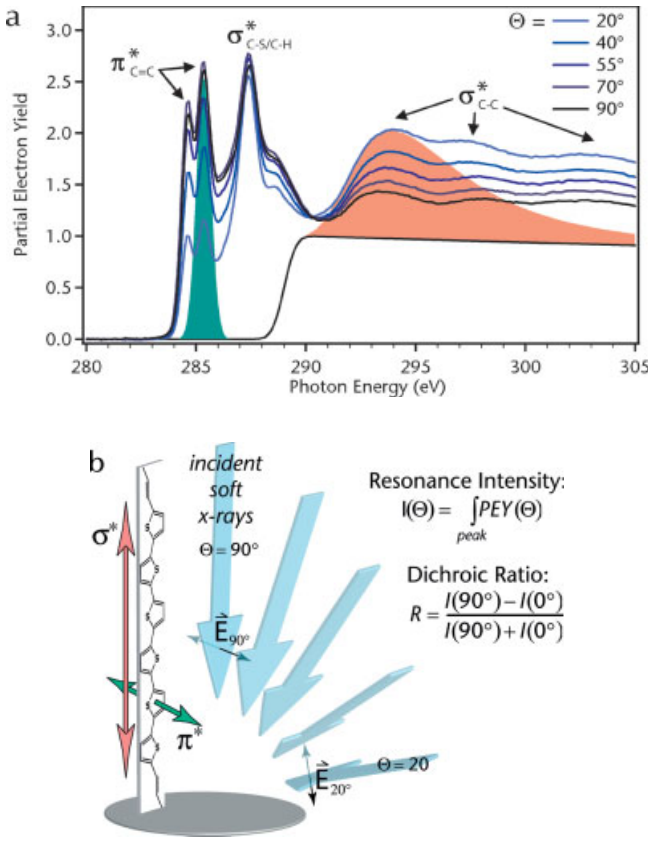

Figure 3. a) NEXAFS carbon K-edge spectra collected at changing incident angles from a film of **2** from thermal treatment at 200 °C. Spectra are normalized to the net carbon signal. The green area indicates the oligothiophene π* resonance used to determine planar orientation while the pink area indicates the σ* resonance used to determine long-axis orientation. b) Image depicting the orientation of **2** and spatial orientations of its primary K-edge carbon resonances. Blue arrows indicate incident polarized soft X-rays with electric field vectors extending normal to the plane of photon polarization. There exists an off-axis component to the σ* resonance of **2** that has been omitted for simplicity.

temperature of 125 °C exceeds the 110 °C melting point observed by differential scanning calorimetry. Second, *R* decreases from 125 °C to 150 °C, indicating that the melt disorder is preserved in cooled films. Third, *R* increases greatly between 150 °C and 200 °C, where the greatest increases in ester thermolysis are also observed, reaching a plateau at 200 °C. At this point, both the conjugated plane and the long axis of the molecule are angled away from the surface. Finally, *R* decreases again at 300 °C, indicating that the molecules are relaxing into a more disordered orientation.

Although we can calculate tilt angles for **2**, they do not describe the lattice tilts of crystals; they are averaged substrate-respective tilts, which is possibly more relevant to hole transport. At 200 °C, the conjugated plane is angled 12° away from the surface normal on average. The long axis appears less oriented because the true carbon–carbon σ* resonance includes off-axis contributions. Analytical vector forms are possible for molecules with simple symmetry,[19,20] but this molecule is complex and a simplified treatment is necessary. The preferential orientation depicted in Figure 3b may possess a slight tilt in the plane or long axis or some distribution in a substrate-relative orientation. Given this orientation, adjacent molecules of **2** could possess either a π–π stacked or herringbone structure in the substrate plane. However, increased vertical order for either packing type should correspond to increased intermolecular π overlap and directly correlate to increased hole mobility. The optimal mobility should be observed within the most vertically oriented regime between 200 °C and 250 °C.

The larger-scale morphology of the semiconductor film is also important because the molecular reorganization that occurs with conversion also causes molecules of **2** to form rough terraces and finally coalesce into islands.[8] During this process, the minimum film thickness decreases and can be quantified with NEXAFS. Further, NEXAFS may be used to detect the eventual formation of film defects. To do this, we measure oxygen K-shell spectra, which exhibit a prominent oxygen–silicon σ* resonance. Comparison of the oxygen–silicon σ* resonance on each sample versus that on bare SiO_2 allows determination of the fraction of organic film within the 6 nm sampling depth, as shown in Figure 1d. A single vertical monolayer of **2** would be 3 nm thick, so monolayer coverage should remain until this organic fraction drops below 50 %.

The onset of reorganization appears at treatment temperatures greater than 150 °C. As the molecules coalesce into tall structures, the film thickness in low areas becomes less than the sampled depth. At 250 °C, the organic fraction indicates a thickness close to a single monolayer. At 300 °C, the organic coverage is less than a monolayer, and defect formation is detected. The surface coverage loss is consistent with the orientation loss at 300 °C, because incomplete packing of surface adsorbed molecules typically leads to a less-vertical orientation.

These three structural aspects quantified by NEXAFS—chemical conversion, molecular ordering, and defect formation—provide a detailed picture that directly correlates to variations in the OFET field-effect mobility over three orders of magnitude. OFET devices were constructed using films fabricated identically to the temperature treatment series measured by NEXAFS. Shadow masks were used to define evaporated-gold top-contact OFETs with channel lengths from 5 to 100 μm. All OFETs were tested in the accumulation regime and saturation hole mobilities were obtained. The variation in field-effect hole mobility with treatment temperature is shown in Figure 1a.

At room temperature, **1** exhibits a field-effect mobility less than 10^{-4} $cm^2 V^{-1} s^{-1}$. At this point **1** is slightly oriented, but is mostly unconverted and retains insulating alkanes. The mobility increases slightly at 150 °C, which is due to the onset of thermolysis to a less-insulating material rather than increased orientation because the molecules are less vertical at this treatment temperature. From 150 °C to 200 °C, the mobility increases dramatically because of the large enhancement in vertical orientation that occurs during conversion. Maximum mobilities of 5×10^{-2} $cm^2 V^{-1} s^{-1}$ are achieved at 200 °C, where

ADVANCED MATERIALS

NEXAFS measurements indicate complete conversion and optimal order. The highest mobilities (for this work) are observed up to 250 °C, even though the film is only slightly more than a monolayer thick by our quantification of surface coverage. The large decrease in mobility at 300 °C can be attributed to defect formation when the thickness becomes submonolayer and film continuity film is lost.

NEXAFS is a powerful, non-destructive technique for the detailed quantification of the structure and chemistry of nanometer-thick organic semiconductor precursor films. This data provides insight and direct correlations with electronic property trends. The sensitivity of NEXAFS to π bonds, its insensitivity to optical quality, and its ability to probe nanoscale films provide an ideal measurement platform for the systematic investigation of organic semiconductors and conductors. From the example given here, the observation that **1** undergoes reorientation during thermolysis suggests that the application of thermal gradients, surface chemical modifications, or mechanical shear may be used to direct preferential organization during conversion. Synthetic improvements might include increasing the solubilizing group volatility or reducing coverage loss at high temperatures by increasing the size of the oligothiophene core. NEXAFS spectroscopy could quantify the structural gains of such strategies. The concurrent development of NEXAFS measurements and new soluble organic semiconductor materials can help accelerate the successful adoption of new processing strategies and applications through the clear correlation of chemistry and physical structure to OFET performance.

Experimental

Materials: All chemicals were purchased from Aldrich and used without further purification unless otherwise noted. Compound **1** was synthesized and characterized as previously described [7].

Transistor Fabrication: OFETs were fabricated atop n-doped silicon wafers with 1250 Å thick thermal silicon dioxide dielectric. Compound **1** was spin-coated at 2000–4000 rpm from 2–3 mg mL^{-1} solutions in anhydrous $CHCl_3$ filtered through 0.2 μm polytetrafluoroethylene filters. Samples were heated on a hot plate in a nitrogen glove box. Gold electrodes were evaporated in a Thermionic evaporator at 5 Å s^{-1} through a shadow mask to a thickness of 500 Å. OFET channels had widths of 200 or 400 μm and lengths from 5 to 40 μm.

NEXAFS Spectroscopy: NEXAFS spectroscopy was performed at the NIST/Dow soft X-ray materials characterization facility at the National Synchrotron Light Source (NSLS) of Brookhaven National Laboratory. Carbon K-edge partial electron yield were collected at a grid bias of –50 V, corresponding to a sampling depth of ≈6 nm. Experimental standard uncertainty in peak position for PEY spectra was ±0.15 eV; yield uncertainly was ±2 %. Oxygen K-edge NEXAFS spectra were collected at an entrance grid bias of –320 V. Six peak shapes were fitted to the carbon spectra. A multivariate secant update (More-Hebdon) was used to minimize the squared error between fit and data. Individual peak shapes included 1) an error function step convoluted to an exponential decay for the ionization edge, 2) Gaussian lineshapes before the ionization edge, and 3) asymmetric Gaussian lineshapes after the ionization edge [21].

Received: February 4, 2005
Final version: May 12, 2005
Published online: August 30, 2005

[1] H. Sirringhaus, N. Tessler, R. H. Friend, *Science* **1998**, *280*, 1741.
[2] H. E. Katz, A. J. Lovinger, J. Johnson, C. Kloc, T. Siegrist, W. Li, Y. Y. Lin, A. Dodabalapur, *Nature* **2000**, *404*, 478.
[3] H. Sirringhaus, T. Kawase, R. H. Friend, T. Shimoda, M. Inbasekaran, W. Wu, E. P. Woo, *Science* **2000**, *290*, 2123.
[4] N. Stutzmann, R. H. Friend, H. Sirringhaus, *Science* **2003**, *299*, 1881.
[5] P. T. Herwig, K. Mullen, *Adv. Mater.* **1999**, *11*, 480.
[6] A. Afzali, C. D. Dimitrakopoulos, T. L. Breen, *J. Am. Chem. Soc.* **2002**, *124*, 8812.
[7] A. R. Murphy, J. M. J. Fréchet, P. Chang, J. Lee, V. Subramanian, *J. Am. Chem. Soc.* **2004**, *126*, 1596.
[8] P. C. Chang, J. Lee, D. Huang, V. Subramanian, A. R. Murphy, J. M. J. Fréchet, *Chem. Mater.* **2004**, *16*, 4783.
[9] J. Stohr, M. G. Samant, J. Luning, A. C. Callegari, P. Chaudhari, J. P. Doyle, J. A. Lacey, S. A. Lien, S. Purushothaman, J. L. Speidell, *Science* **2001**, *292*, 2299.
[10] D. A. Fischer, J. Colbert, J. L. Gland, *Rev. Sci. Instrum.* **1989**, *60*, 1596.
[11] J. Stöhr, *NEXAFS Spectroscopy*, Springer Series in Surface Sciences, Vol. 392, Springer, Berlin **1992**.
[12] A. Dodabalapur, L. Torsi, H. E. Katz, *Science* **1995**, *268*, 270.
[13] J. Stohr, J. L. Gland, E. B. Kollin, R. J. Koestner, A. L. Johnson, E. L. Muetterties, F. Sette, *Phys. Rev. Lett.* **1984**, *53*, 2161.
[14] A. P. Hitchcock, J. A. Horsley, J. Stöhr, *J. Chem. Phys.* **1986**, *85*, 4835.
[15] G. Tourillon, E. Dartyge, A. Fontaine, R. Garrett, M. Sagurton, P. Xu, G. P. Williams, *Europhys. Lett.* **1987**, *4*, 1391.
[16] S. G. Urquhart, H. Ade, *J. Phys. Chem. B* **2002**, *106*, 8531.
[17] W. E. Wallace, D. A. Fischer, K. Efimenko, W. L. Wu, J. Genzer, *Macromolecules* **2001**, *34*, 5081.
[18] W. L. Wu, S. Sambasivan, C. Y. Wang, W. E. Wallace, J. Genzer, D. A. Fischer, *Eur. Phys. J. E* **2003**, *12*, 127.
[19] J. Genzer, E. J. Kramer, D. A. Fischer, *J. Appl. Phys.* **2002**, *92*, 7070.
[20] D. A. Outka, J. Stöhr, J. P. Rabe, J. D. Swalen, *J. Chem. Phys.* **1988**, *88*, 4076.
[21] D. A. Outka, J. Stöhr, *J. Chem. Phys.* **1988**, *88*, 3539.

Dynamic Tuning of Photoluminescent Dyes in Crystalline Colloidal Arrays**

By *Justin R. Lawrence*, *Goo Hwan Shim*, *Ping Jiang*, *Moon Gyu Han*, *Yurong Ying*, and *Stephen H. Foulger**

Recent widespread application of colloidal crystals in materials research has attempted to gain fundamental insights into colloidal forces and self-assembly, in addition to providing precursors for the next generation of advanced materials.[1,2]

[*] Prof. S. H. Foulger, Dr. J. R. Lawrence, G. H. Shim, Dr. P. Jiang, Dr. M. G. Han, Y. Ying
Center for Optical Materials Science and Engineering Technologies
School of Materials Science and Engineering
Clemson University, Clemson, SC 29634-0971 (USA)
E-mail: foulger@clemson.edu

[**] The authors thank DARPA (grant no. N66001-04-1-8933) and the National Science Foundation through a CAREER award (grant no. DMR-0236692) (SHF) for financial support.

  DOI: 10.1002/adma.200500617